Available online at www.sciencedirect.com

ScienceDirect

Physics Letters B 663 (2008) 26–36

PHYSICS LETTERS B

www.elsevier.com/locate/physletb

A combined search for the standard model Higgs boson at $\sqrt{s} = 1.96$ TeV

DØ Collaboration

V.M. Abazov [aj], B. Abbott [bx], M. Abolins [bn], B.S. Acharya [ac], M. Adams [az], T. Adams [ax], E. Aguilo [f], S.H. Ahn [ae], M. Ahsan [bh], G.D. Alexeev [aj], G. Alkhazov [an], A. Alton [bm,1], G. Alverson [bl], G.A. Alves [b], M. Anastasoaie [ai], L.S. Ancu [ai], T. Andeen [bb], S. Anderson [at], B. Andrieu [q], M.S. Anzelc [bb], Y. Arnoud [n], M. Arov [bi], M. Arthaud [r], A. Askew [ax], B. Åsman [ao], A.C.S. Assis Jesus [c], O. Atramentov [ax], C. Autermann [u], C. Avila [h], C. Ay [x], F. Badaud [m], A. Baden [bj], L. Bagby [ba], B. Baldin [ay], S. Banerjee [ac], P. Banerjee [ac], E. Barberis [bl], A.-F. Barfuss [o], P. Bargassa [cc], P. Baringer [bg], J. Barreto [b], J.F. Bartlett [ay], U. Bassler [r], D. Bauer [ar], S. Beale [f], A. Bean [bg], M. Begalli [c], M. Begel [bt], C. Belanger-Champagne [ao], L. Bellantoni [ay], A. Bellavance [ay], J.A. Benitez [bn], S.B. Beri [aa], G. Bernardi [q,*], R. Bernhard [w], I. Bertram [aq], M. Besançon [r], R. Beuselinck [ar], V.A. Bezzubov [am], P.C. Bhat [ay], V. Bhatnagar [aa], C. Biscarat [t], G. Blazey [ba], F. Blekman [ar], S. Blessing [ax], D. Bloch [s], K. Bloom [bp], A. Boehnlein [ay], D. Boline [bk], T.A. Bolton [bh], G. Borissov [aq], T. Bose [bz], A. Brandt [ca], R. Brock [bn], G. Brooijmans [bs], A. Bross [ay], D. Brown [cd], N.J. Buchanan [ax], D. Buchholz [bb], M. Buehler [cd], V. Buescher [v], V. Bunichev [al], S. Burdin [aq,2], S. Burke [at], T.H. Burnett [ce], C.P. Buszello [ar], J.M. Butler [bk], P. Calfayan [y], S. Calvet [p], J. Cammin [bt], W. Carvalho [c], B.C.K. Casey [ay], N.M. Cason [bd], H. Castilla-Valdez [ag], S. Chakrabarti [r], D. Chakraborty [ba], K.M. Chan [bd], K. Chan [f], A. Chandra [aw], F. Charles [s,✠], E. Cheu [at], F. Chevallier [n], D.K. Cho [bk], S. Choi [af], B. Choudhary [ab], L. Christofek [bz], T. Christoudias [ar,3], S. Cihangir [ay], D. Claes [bp], Y. Coadou [f], M. Cooke [cc], W.E. Cooper [ay], M. Corcoran [cc], F. Couderc [r], M.-C. Cousinou [o], S. Crépé-Renaudin [n], D. Cutts [bz], M. Ćwiok [ad], H. da Motta [b], A. Das [at], G. Davies [ar], K. De [ca], S.J. de Jong [ai], E. De La Cruz-Burelo [bm], C. De Oliveira Martins [c], J.D. Degenhardt [bm], F. Déliot [r], M. Demarteau [ay], R. Demina [bt], D. Denisov [ay], S.P. Denisov [am], S. Desai [ay], H.T. Diehl [ay], M. Diesburg [ay], A. Dominguez [bp], H. Dong [bu], L.V. Dudko [al], L. Duflot [p], S.R. Dugad [ac], D. Duggan [ax], A. Duperrin [o], J. Dyer [bn], A. Dyshkant [ba], M. Eads [bp], D. Edmunds [bn], J. Ellison [aw], J. Elmsheuser [y], V.D. Elvira [ay], Y. Enari [bz], S. Eno [bj], P. Ermolov [al], H. Evans [bc], A. Evdokimov [bv], V.N. Evdokimov [am], A.V. Ferapontov [bh], T. Ferbel [bt], F. Fiedler [x], F. Filthaut [ai], W. Fisher [ay], H.E. Fisk [ay], M. Ford [as], M. Fortner [ba], H. Fox [w], S. Fu [ay], S. Fuess [ay], T. Gadfort [ce], C.F. Galea [ai], E. Gallas [ay], E. Galyaev [bd], C. Garcia [bt], A. Garcia-Bellido [ce], V. Gavrilov [ak], P. Gay [m], W. Geist [s], D. Gelé [s], C.E. Gerber [az], Y. Gershtein [ax], D. Gillberg [f], G. Ginther [bt], N. Gollub [ao], B. Gómez [h], A. Goussiou [bd], P.D. Grannis [bu], H. Greenlee [ay], Z.D. Greenwood [bi], E.M. Gregores [d], G. Grenier [t], Ph. Gris [m], J.-F. Grivaz [p], A. Grohsjean [y], S. Grünendahl [ay], M.W. Grünewald [ad], J. Guo [bu], F. Guo [bu], P. Gutierrez [bx], G. Gutierrez [ay], A. Haas [bs], N.J. Hadley [bj], P. Haefner [y], S. Hagopian [ax], J. Haley [bq], I. Hall [bn], R.E. Hall [av], L. Han [g], K. Hanagaki [ay], P. Hansson [ao], K. Harder [as], A. Harel [bt], R. Harrington [bl], J.M. Hauptman [bf], R. Hauser [bn], J. Hays [ar], T. Hebbeker [u], D. Hedin [ba], J.G. Hegeman [ah], J.M. Heinmiller [az], A.P. Heinson [aw], U. Heintz [bk], C. Hensel [bg], K. Herner [bu], G. Hesketh [bl],

0370-2693/$ – see front matter
doi:10.1016/j.physletb.2008.02.069

M.D. Hildreth [bd], R. Hirosky [cd], J.D. Hobbs [bu], B. Hoeneisen [l], H. Hoeth [z], M. Hohlfeld [v], S.J. Hong [ae], S. Hossain [bx], P. Houben [ah], Y. Hu [bu], Z. Hubacek [j], V. Hynek [i], I. Iashvili [br], R. Illingworth [ay], A.S. Ito [ay], S. Jabeen [bk], M. Jaffré, [p] S. Jain [bx], K. Jakobs [w], C. Jarvis [bj], R. Jesik [ar], K. Johns [at], C. Johnson [bs], M. Johnson [ay], A. Jonckheere [ay], P. Jonsson [ar], A. Juste [ay], D. Käfer [u], E. Kajfasz [o], A.M. Kalinin [aj], J.R. Kalk [bn], J.M. Kalk [bi], S. Kappler [u], D. Karmanov [al], P. Kasper [ay], I. Katsanos [bs], D. Kau [ax], R. Kaur [aa], V. Kaushik [ca], R. Kehoe [cb], S. Kermiche [o], N. Khalatyan [ay], A. Khanov [by], A. Kharchilava [br], Y.M. Kharzheev [aj], D. Khatidze [bs], H. Kim [af], T.J. Kim [ae], M.H. Kirby [bb], M. Kirsch [u], B. Klima [ay], J.M. Kohli [aa], J.-P. Konrath [w], M. Kopal [bx], V.M. Korablev [am], A.V. Kozelov [am], D. Krop [bc], T. Kuhl [x], A. Kumar [br], S. Kunori [bj], A. Kupco [k], T. Kurča [t], J. Kvita [i], F. Lacroix [m], D. Lam [bd], S. Lammers [bs], G. Landsberg [bz], P. Lebrun [t], W.M. Lee [ay], A. Leflat [al], F. Lehner [ap], J. Lellouch [q], J. Leveque [at], P. Lewis [ar], J. Li [ca], Q.Z. Li [ay], L. Li [aw], S.M. Lietti [e], J.G.R. Lima [ba], D. Lincoln [ay], J. Linnemann [bn], V.V. Lipaev [am], R. Lipton [ay], Y. Liu [g,3], Z. Liu [f], L. Lobo [ar], A. Lobodenko [an], M. Lokajicek [k], P. Love [aq], H.J. Lubatti [ce], A.L. Lyon [ay], A.K.A. Maciel [b], D. Mackin [cc], R.J. Madaras [au], P. Mättig [z], C. Magass [u], A. Magerkurth [bm], P.K. Mal [bd], H.B. Malbouisson [c], S. Malik [bp], V.L. Malyshev [aj], H.S. Mao [ay], Y. Maravin [bh], B. Martin [n], R. McCarthy [bu], A. Melnitchouk [bo], A. Mendes [o], L. Mendoza [h], P.G. Mercadante [e], M. Merkin [al], K.W. Merritt [ay], J. Meyer [v,4], A. Meyer [u], T. Millet [t], J. Mitrevski [bs], J. Molina [c], R.K. Mommsen [as], N.K. Mondal [ac], R.W. Moore [f], T. Moulik [bg], G.S. Muanza [t], M. Mulders [ay], M. Mulhearn [bs], O. Mundal [v], L. Mundim [c], E. Nagy [o], M. Naimuddin [ay], M. Narain [bz], N.A. Naumann [ai], H.A. Neal [bm], J.P. Negret [h], P. Neustroev [an], H. Nilsen [w], H. Nogima [c], A. Nomerotski [ay], S.F. Novaes [e], T. Nunnemann [y], V. O'Dell [ay], D.C. O'Neil [f], G. Obrant [an], C. Ochando [p], D. Onoprienko [bh], N. Oshima [ay], J. Osta [bd], R. Otec [j], G.J. Otero y Garzón [ay], M. Owen [as], P. Padley [cc], M. Pangilinan [bz], N. Parashar [be], S.-J. Park [bt], S.K. Park [ae], J. Parsons [bs], R. Partridge [bz], N. Parua [bc], A. Patwa [bv], G. Pawloski [cc], B. Penning [w], M. Perfilov [al], K. Peters [as], Y. Peters [z], P. Pétroff [p], M. Petteni [ar], R. Piegaia [a], J. Piper [bn], M.-A. Pleier [v], P.L.M. Podesta-Lerma [ag,5], V.M. Podstavkov [ay], Y. Pogorelov [bd], M.-E. Pol [b], P. Polozov [ak], B.G. Pope [bn], A.V. Popov [am], C. Potter [f], W.L. Prado da Silva [c], H.B. Prosper [ax], S. Protopopescu [bv], J. Qian [bm], A. Quadt [v,4], B. Quinn [bo], A. Rakitine [aq], M.S. Rangel [b], K. Ranjan [ab], P.N. Ratoff [aq], P. Renkel [cb], S. Reucroft [bl], P. Rich [as], M. Rijssenbeek [bu], I. Ripp-Baudot [s], F. Rizatdinova [by], S. Robinson [ar], R.F. Rodrigues [c], M. Rominsky [bx], C. Royon [r], P. Rubinov [ay], R. Ruchti [bd], G. Safronov [ak], G. Sajot [n], A. Sánchez-Hernández [ag], M.P. Sanders [q], A. Santoro [c], G. Savage [ay], L. Sawyer [bi], T. Scanlon [ar], D. Schaile [y], R.D. Schamberger [bu], Y. Scheglov [an], H. Schellman [bb], P. Schieferdecker [y], T. Schliephake [z], C. Schwanenberger [as], A. Schwartzman [bq], R. Schwienhorst [bn], J. Sekaric [ax], H. Severini [bx], E. Shabalina [az], M. Shamim [bh], V. Shary [r], A.A. Shchukin [am], R.K. Shivpuri [ab], V. Siccardi [s], V. Simak [j], V. Sirotenko [ay], P. Skubic [bx], P. Slattery [bt], D. Smirnov [bd], J. Snow [bw], G.R. Snow [bp], S. Snyder [bv], S. Söldner-Rembold [as], L. Sonnenschein [q], A. Sopczak [aq], M. Sosebee [ca], K. Soustruznik [i], M. Souza [b], B. Spurlock [ca], J. Stark [n], J. Steele [bi], V. Stolin [ak], D.A. Stoyanova [am], J. Strandberg [bm], S. Strandberg [ao], M.A. Strang [br], M. Strauss [bx], E. Strauss [bu], R. Ströhmer [y], D. Strom [bb], L. Stutte [ay], S. Sumowidagdo [ax], P. Svoisky [bd], A. Sznajder [c], M. Talby [o], P. Tamburello [at], A. Tanasijczuk [a], W. Taylor [f], J. Temple [at], B. Tiller [y], F. Tissandier [m], M. Titov [r], V.V. Tokmenin [aj], T. Toole [bj], I. Torchiani [w], T. Trefzger [x], D. Tsybychev [bu], B. Tuchming [r], C. Tully [bq], P.M. Tuts [bs], R. Unalan [bn], S. Uvarov [an], L. Uvarov [an], S. Uzunyan [ba], B. Vachon [f], P.J. van den Berg [ah], R. Van Kooten [bc], W.M. van Leeuwen [ah], N. Varelas [az], E.W. Varnes [at], I.A. Vasilyev [am], M. Vaupel [z], P. Verdier [t], L.S. Vertogradov [aj], M. Verzocchi [ay], F. Villeneuve-Seguier [ar], P. Vint [ar], P. Vokac [j], E. Von Toerne [bh], M. Voutilainen [bp,6], R. Wagner [bq], H.D. Wahl [ax], L. Wang [bj], M.H.L.S. Wang [ay],

J. Warchol [bd], G. Watts [ce], M. Wayne [bd], M. Weber [ay], G. Weber [x], A. Wenger [w,7], N. Wermes [v], M. Wetstein [bj], A. White [ca], D. Wicke [z], G.W. Wilson [bg], S.J. Wimpenny [aw], M. Wobisch [bi], D.R. Wood [bl], T.R. Wyatt [as], Y. Xie [bz], S. Yacoob [bb], R. Yamada [ay], M. Yan [bj], T. Yasuda [ay], Y.A. Yatsunenko [aj], K. Yip [bv], H.D. Yoo [bz], S.W. Youn [bb], J. Yu [ca], A. Zatserklyaniy [ba], C. Zeitnitz [z], T. Zhao [ce], B. Zhou [bm], J. Zhu [bu], M. Zielinski [bt], D. Zieminska [bc,✠], A. Zieminski [bc], L. Zivkovic [bs], V. Zutshi [ba], E.G. Zverev [al]

[a] *Universidad de Buenos Aires, Buenos Aires, Argentina*
[b] *LAFEX, Centro Brasileiro de Pesquisas Físicas, Rio de Janeiro, Brazil*
[c] *Universidade do Estado do Rio de Janeiro, Rio de Janeiro, Brazil*
[d] *Universidade Federal do ABC, Santo André, Brazil*
[e] *Instituto de Física Teórica, Universidade Estadual Paulista, São Paulo, Brazil*
[f] *University of Alberta, Edmonton, Alberta, and Simon Fraser University, Burnaby, British Columbia, and York University, Toronto, Ontario, and McGill University, Montreal, Quebec, Canada*
[g] *University of Science and Technology of China, Hefei, People's Republic of China*
[h] *Universidad de los Andes, Bogotá, Colombia*
[i] *Center for Particle Physics, Charles University, Prague, Czech Republic*
[j] *Czech Technical University, Prague, Czech Republic*
[k] *Center for Particle Physics, Institute of Physics, Academy of Sciences of the Czech Republic, Prague, Czech Republic*
[l] *Universidad San Francisco de Quito, Quito, Ecuador*
[m] *Laboratoire de Physique Corpusculaire, IN2P3-CNRS, Université Blaise Pascal, Clermont-Ferrand, France*
[n] *Laboratoire de Physique Subatomique et de Cosmologie, IN2P3-CNRS, Universite de Grenoble 1, Grenoble, France*
[o] *CPPM, IN2P3-CNRS, Université de la Méditerranée, Marseille, France*
[p] *Laboratoire de l'Accélérateur Linéaire, IN2P3-CNRS et Université Paris-Sud, Orsay, France*
[q] *LPNHE, IN2P3-CNRS, Universités Paris VI and VII, Paris, France*
[r] *DAPNIA/Service de Physique des Particules, CEA, Saclay, France*
[s] *IPHC, Université Louis Pasteur et Université de Haute Alsace, CNRS, IN2P3, Strasbourg, France*
[t] *IPNL, Université Lyon 1, CNRS/IN2P3, Villeurbanne, France and Université de Lyon, Lyon, France*
[u] *III. Physikalisches Institut A, RWTH Aachen, Aachen, Germany*
[v] *Physikalisches Institut, Universität Bonn, Bonn, Germany*
[w] *Physikalisches Institut, Universität Freiburg, Freiburg, Germany*
[x] *Institut für Physik, Universität Mainz, Mainz, Germany*
[y] *Ludwig-Maximilians-Universität München, München, Germany*
[z] *Fachbereich Physik, University of Wuppertal, Wuppertal, Germany*
[aa] *Panjab University, Chandigarh, India*
[ab] *Delhi University, Delhi, India*
[ac] *Tata Institute of Fundamental Research, Mumbai, India*
[ad] *University College Dublin, Dublin, Ireland*
[ae] *Korea Detector Laboratory, Korea University, Seoul, South Korea*
[af] *SungKyunKwan University, Suwon, South Korea*
[ag] *CINVESTAV, Mexico City, Mexico*
[ah] *FOM-Institute NIKHEF and University of Amsterdam/NIKHEF, Amsterdam, The Netherlands*
[ai] *Radboud University Nijmegen/NIKHEF, Nijmegen, The Netherlands*
[aj] *Joint Institute for Nuclear Research, Dubna, Russia*
[ak] *Institute for Theoretical and Experimental Physics, Moscow, Russia*
[al] *Moscow State University, Moscow, Russia*
[am] *Institute for High Energy Physics, Protvino, Russia*
[an] *Petersburg Nuclear Physics Institute, St. Petersburg, Russia*
[ao] *Lund University, Lund, and Royal Institute of Technology and Stockholm University, Stockholm, and Uppsala University, Uppsala, Sweden*
[ap] *Physik Institut der Universität Zürich, Zürich, Switzerland*
[aq] *Lancaster University, Lancaster, United Kingdom*
[ar] *Imperial College, London, United Kingdom*
[as] *University of Manchester, Manchester, United Kingdom*
[at] *University of Arizona, Tucson, AZ 85721, USA*
[au] *Lawrence Berkeley National Laboratory and University of California, Berkeley, CA 94720, USA*
[av] *California State University, Fresno, CA 93740, USA*
[aw] *University of California, Riverside, CA 92521, USA*
[ax] *Florida State University, Tallahassee, FL 32306, USA*
[ay] *Fermi National Accelerator Laboratory, Batavia, IL 60510, USA*
[az] *University of Illinois at Chicago, Chicago, IL 60607, USA*
[ba] *Northern Illinois University, DeKalb, IL 60115, USA*
[bb] *Northwestern University, Evanston, UL 60208, USA*
[bc] *Indiana University, Bloomington, IN 47405, USA*
[bd] *University of Notre Dame, Notre Dame, IN 46556, USA*
[be] *Purdue University Calumet, Hammond, IN 46323, USA*

[bf] Iowa State University, Ames, IA 50011, USA
[bg] University of Kansas, Lawrence, KS 66045, USA
[bh] Kansas State University, Manhattan, KS 66506, USA
[bi] Louisiana Tech University, Ruston, LA 71272, USA
[bj] University of Maryland, College Park, MD 20742, USA
[bk] Boston University, Boston, MA 02215, USA
[bl] Northeastern University, Boston, MA 02115, USA
[bm] University of Michigan, Ann Arbor, MI 48109, USA
[bn] Michigan State University, East Lansing, MI 48824, USA
[bo] University of Mississippi, University, MS 38677, USA
[bp] University of Nebraska, Lincoln, NE 68588, USA
[bq] Princeton University, Princeton, NJ 08544, USA
[br] State University of New York, Buffalo, NY 14260, USA
[bs] Columbia University, New York, NY 10027, USA
[bt] University of Rochester, Rochester, NY 14627, USA
[bu] State University of New York, Stony Brook, NY 11794, USA
[bv] Brookhaven National Laboratory, Upton, NY 11973, USA
[bw] Langston University, Langston, OK 73050, USA
[bx] University of Oklahoma, Norman, OK 73019, USA
[by] Oklahoma State University, Stillwater, OK 74078, USA
[bz] Brown University, Providence, RI 02912, USA
[ca] University of Texas, Arlington, TX 76019, USA
[cb] Southern Methodist University, Dallas, TX 75275, USA
[cc] Rice University, Houston, TX 77005, USA
[cd] University of Virginia, Charlottesville, VA 22901, USA
[ce] University of Washington, Seattle, WA 98195, USA

Received 5 December 2007; received in revised form 28 January 2008; accepted 7 February 2008

Available online 29 March 2008

Editor: L. Rolandi

Abstract

We present new results of the search for $WH \to \ell\nu b\bar{b}$ production in $p\bar{p}$ collisions at a center-of-mass energy of $\sqrt{s} = 1.96$ TeV, based on a dataset with integrated luminosity of 0.44 fb^{-1}. We combine these new results with previously published searches by the D0 collaboration, for WH and ZH production analyzed in the $\not\!\!E_T b\bar{b}$ final state, for ZH ($\to \ell^+\ell^- b\bar{b}$) production, for WH ($\to WWW$) production, and for H ($\to WW$) direct production. No signal-like excess is observed either in the WH analysis or in the combination of all D0 Higgs boson analyses. We set 95% C.L. (expected) upper limits on $\sigma(p\bar{p} \to WH) \times B(H \to b\bar{b})$ ranging from 1.6 (2.2) pb to 1.9 (3.3) pb for Higgs boson masses between 105 and 145 GeV, to be compared to the theoretical prediction of 0.13 pb for a Standard Model (SM) Higgs boson with mass $m_H = 115$ GeV. After combination with the other D0 Higgs boson searches, we obtain for $m_H = 115$ GeV an observed (expected) limit 8.5 (12.1) times higher than the SM predicted Higgs boson production cross section. For $m_H = 160$ GeV, the corresponding observed (expected) ratio is 10.2 (9.0).

PACS: 13.85Qk; 13.85.Rm

Spontaneous electroweak symmetry breaking in the Standard Model (SM) provides an explanation for the masses of the elementary particles, otherwise massless in the unbroken gauge theory. Its success, in particular in explaining the mass of the electroweak vector bosons, awaits one last but necessary experimental confirmation: the observation of the Higgs boson, which is a scalar particle associated with the symmetry breaking. For Higgs boson searches, the most sensitive production channel at the Tevatron for a Higgs boson with mass below 130 GeV is the associated production of a Higgs boson with a W boson. All possible channels, however, must be studied to gain sensitivity through their combination.

At a center-of-mass energy of $\sqrt{s} = 1.96$ TeV, three $p\bar{p} \to WH$ searches have already been published, one [1] using a subsample (0.17 fb^{-1}) of the dataset used in this letter, while the two others are from the CDF collaboration: one uses 0.32 fb^{-1} [2] of data, the other updates it using improved analysis techniques and a larger dataset based on 1.0 fb^{-1} of integrated luminosity [3].

* Corresponding author.
E-mail address: gregorio@in2p3.fr (G. Bernardi).
[1] Visitor from Augustana College, Sioux Falls, SD, USA.
[2] Visitor from The University of Liverpool, Liverpool, UK.
[3] Fermilab International Fellow.
[4] Visitor from II. Physikalisches Institut, Georg-August-University Göttingen, Germany.
[5] Visitor from ICN-UNAM, Mexico City, Mexico.
[6] Visitor from Helsinki Institute of Physics, Helsinki, Finland.
[7] Visitor from Universität Zürich, Zürich, Switzerland.
✠ Deceased.

For this WH analysis we require one high transverse momentum (p_T) lepton (e or μ), missing transverse energy $\not\!\!E_T$ to account for the neutrino in the W boson decay, and exactly two jets with at least one of them being identified as originating from a bottom (b) quark jet ("b-tagged"), as detailed below. The dominant backgrounds to WH production are $W+$ heavy-flavor production, top quark pair production ($t\bar{t}$), and single top quark production. This analysis uses a dataset of 0.44 fb^{-1}. Compared to the previous D0 result, the b-jet identification has been optimized, and the muon channel has been added.

The result of this search is then combined with previously published searches by the D0 Collaboration with a similar luminosity. These searches cover WH and ZH production analyzed in the $\not\!\!E_T b\bar{b}$ final state [4], ZH ($\rightarrow \ell^+\ell^- b\bar{b}$) production [5], WH ($\rightarrow WW^+W^-$) production [6], and H ($\rightarrow W^+W^-$) direct production [7]. In the following, the particle charges will not be mentioned explicitly, except when needed to resolve potential ambiguity. We first describe the WH analysis in detail, then the full combination of results. Note that the results of Refs. [4,6] and [7] have been updated for this combination to take into account the change in luminosity measurement at DØ, as described in Ref. [8].

The WH analysis relies on the following components of the D0 detector [9,10]:

(i) a central-tracking system, which consists of a silicon microstrip tracker (SMT) and a central fiber tracker, both located within a 2 T superconducting solenoidal magnet;

(ii) a liquid-argon/uranium calorimeter with a central action (CC) covering pseudorapidity[8] $|\eta| < 1.1$, and two end calorimeters (EC) extending coverage to $|\eta| \simeq 3.2$, all housed in separate cryostats, and with scintillators between the CC and EC cryostats providing sampling of developing showers at $1.1 < |\eta| < 1.4$;

(iii) a muon system, which surrounds the calorimeter and consists of a layer of tracking detectors and scintillation trigger counters before 1.8 T iron toroids, followed by two more similar layers behind the toroids.

We reject data periods in which the quality of the data in the tracking, the calorimeter, or the muon system is compromised. The luminosity is measured using plastic scintillator arrays located in front of the EC cryostats, covering $2.7 < |\eta| < 4.4$. The uncertainty on the measured luminosity is 6.1%. The $W+$ jets candidate events must pass one of the triggers which require, for the e channel, at least one electromagnetic (EM) object, and for the μ channel, at least one muon object or a trigger requiring a muon and a jet in the final state.

The event selection for the WH analysis requires one lepton candidate with transverse momentum $p_T > 20$ GeV, $\not\!\!E_T > 25$ GeV, and exactly two jets with $p_T > 20$ GeV and $|\eta| < 2.5$. Only events having a primary z vertex within ± 60 cm of the nominal interaction point are accepted. If the lepton is an electron, it is required to have $|\eta| < 1.1$. If it is a muon the requirement is $|\eta| < 2.0$.

[8] The pseudorapidity is defined as a function of the polar angle θ as $\eta \equiv -\ln(\tan\frac{\theta}{2})$.

Electrons are identified in two steps. The preselected electron candidates (seeded by an energy cluster in the EM calorimeter) are first required to satisfy identification (ID) criteria: (a) a large fraction of their energy deposited in EM layers, i.e., EMF > 0.9, (b) low fractional energy deposited around the expected electron energy deposition, and (c) spatial energy distribution in the EM calorimeter consistent with that of an electron. These criteria define "loose" electrons. The loose electrons are then tested with a likelihood algorithm, optimized on $Z \rightarrow ee$ samples, and which takes as input seven quantities sensitive to the EM nature of the particles [11]. If they satisfy the likelihood requirement, they are accepted as final ("tight") electrons for the analysis. The efficiencies of the ID and likelihood requirements are determined from a dielectron sample in which we select a pure set of Z events. The combined reconstruction and ID efficiency is found to be $(95.4 \pm 0.4)\%$. The likelihood efficiency for electrons is $(92.0 \pm 0.3)\%$.

Muons are reconstructed using information from the muon detector and the central tracker. They are required to have hits in all layers of the muon system inside and outside the toroid. The superior spatial resolution of the central tracker, inside the strong solenoidal magnetic field, is used to improve the accuracy of kinematic properties of the muon and to confirm that the muon originated from the primary vertex. A veto against cosmic-ray muons based on the timing of hits in the muon-system scintillator detectors is applied. Quality criteria on the associated central track are also applied to reject the majority of background muons: a small track impact parameter (dca) compared to its resolution ($\sigma_{\rm dca}$) is required, dca $< 3\sigma_{\rm dca}$, to reject muons originating from semi-leptonic decays of heavy-flavor hadrons which constitute the main background. Such background muons have a lower transverse momentum spectrum and are not typically isolated due to jet fragmentation. A loose isolation criterion is defined using the spatial separation $\Delta R = \sqrt{(\Delta\eta)^2 + (\Delta\varphi)^2}$ between a muon and the closest jet in the η–φ plane, where φ is the azimuthal angle, we require $\Delta R > 0.5$. Tighter muon isolation criteria are defined by requiring that the scalar sum of the transverse energy of calorimeter clusters in a hollow cone ($0.1 < \Delta R < 0.4$) around the muon divided by the p_T of the muon be less than 0.08, and the scalar sum of the transverse momenta of all tracks within a cone of radius $\Delta R = 0.5$ around the muon divided by the p_T of the muon be less than 0.06. The track matched to the muon is excluded from this sum.

The jets are reconstructed using a cone algorithm [18] with a radius of $\Delta R = 0.5$. We apply standard D0 jet-ID criteria to avoid fake jets which occasionally originate from noise in the calorimeter, i.e., the energy fraction in the EM layers of a jet is required to be $0.05 <$ EMF < 0.95 and the energy fraction in the CH section of the calorimeter is required to be < 0.4. The difference in efficiency of the jet-ID requirements between data and simulation is quantified in the overall jet reconstruction efficiency scale factor to which a systematic uncertainty of 5% (per jet) is assigned.

The multijet background is estimated from the loose and tight e or μ final samples. as described in Ref. [11] using the following probabilities. We determine from the data the proba-

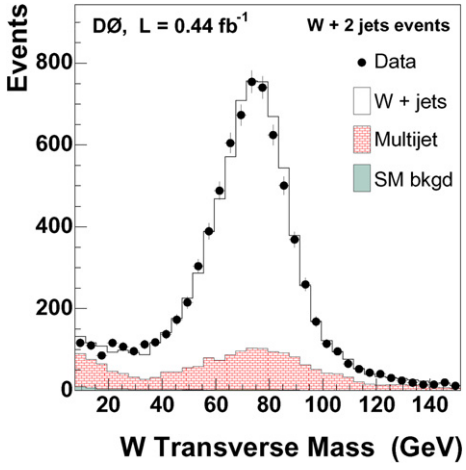

Fig. 1. Distributions of the transverse W boson mass compared to the simulated expectation in the $W+2$ jet event sample. The simulation is normalized to the integrated luminosity of the data sample using the expected cross sections taking into account all the other backgrounds (the fraction of WH events is negligible before b-tagging).

bility $p^{\text{multijet}}_{\text{loose}\to\text{tight}}$ for a "loose" lepton originating from a jet to pass the tight lepton requirements. This is done separately for the electron and the muon channel and this probability is determined as a function of the p_T of the candidate lepton. The sample of multijet events containing a loose lepton is selected with kinematic criteria that ensure negligible contamination of real leptons. We also determine the same type of probability $p^{\text{signal}}_{\text{loose}\to\text{tight}}$ for a genuine isolated lepton from $Z\to\ell^+\ell^-$ samples. With these two probabilities and the numbers of loose and tight $W+2$ jet candidates, we determine the number of multijet background events in our sample, bin-by-bin, for every differential distribution.

To select W boson decays, we require $\not\!\!E_T > 25$ GeV. The $\not\!\!E_T$ is calculated from the calorimeter cells except for unclustered cells in the outermost layer of the calorimeter (coarse hadronic layer, CH) and is corrected when one or several muons are present. All energy corrections to electrons or jets are also propagated into the $\not\!\!E_T$. The transverse mass of the W boson candidates in the $W+$ jets sample is reconstructed from the lepton and missing transverse energies. Its distribution is shown in Fig. 1 and compared with the sum of contributions from multijet events with misidentified leptons and from SM processes which are obtained from simulated events.

The following processes are simulated with the PYTHIA [12] MC event generator version 6.202, making use of the CTEQ5L [13] leading-order parton distribution functions: inclusive production of $W\to e/\mu/\tau+\nu$; $Z\to ee/\mu\mu/\tau\tau$; WW, WZ, ZZ; $t\bar{t}\to e/\mu/\tau+$jets production (lepton + jets and dilepton channels), $WH\to e/\mu/\tau+\nu+b\bar{b}$ production. The single top quark processes are generated using COMPHEP [14].

Throughout this Letter, "$W+$jets" simulated events refer to events with a W produced in association with light-flavor jets (originating from u, d, s quarks or gluons; generically denoted by j) or charm jets (originating from a c quark). They constitute the dominant background before b-tagging and are generated with ALPGEN [15] (interfaced to PYTHIA for showering and fragmentation), since ALPGEN has a more complete simulation of processes with high jet multiplicities. The generation is based on $W+2$ jets (Wjj) processes, including the charm quark (c) processes $Wc\bar{c}$ and Wcj. The $Wb\bar{b}$ events are generated separately requiring two b parton jets with $p_T > 8$ GeV separated by $\Delta R > 0.4$; its NLO cross section is obtained using MCFM [16].

These simulated backgrounds are absolutely normalized (according to NLO cross sections) with the exception of the $W+$ jets sample which is normalized to the data after subtraction of all the other backgrounds. The systematic uncertainty on the NLO cross sections of these processes is 6–18%, depending on the process. All these events are processed through the D0 detector simulation, based on GEANT [17], and the reconstruction software. The simulated events are then weighted by the trigger efficiency and by the data/simulation ratio of all the selection efficiencies. The shape of the distribution of the transverse mass of the W candidates (Fig. 1) is well reproduced by the simulation of the $W+$ jets processes, after adding the multijet background and the other SM backgrounds.

To identify heavy-flavor jets we use a b-tagging algorithm which computes a probability correlated to the b quark lifetime [19]. The requirements on the "jet lifetime probability" (JLIP) have been optimized for events with one or two b-jet candidates by maximizing the sensitivity to the Higgs boson signal. The requirement is first set to 1%; if two jets are tagged the event is selected as double b-tagged (DT). Otherwise the requirement is tightened to 0.1% and if exactly one jet is tagged the event is selected as single b-tagged (ST). In this way the single and double b-tagged subsamples are independent, which simplifies their combination. The mistag rate (tagging of light flavor jets) obtained in these samples are approximately equal to the corresponding JLIP requirements, while the efficiency for correctly identifying a genuine b jet ("b-tagging efficiency") is $(55\pm4)\%$ and $(33\pm4)\%$, respectively. These efficiencies were determined with central "taggable" jets ($|\eta|<1.2$) having a transverse momentum of $35 < p_T < 55$ GeV. A jet is "taggable" if at least 2 tracks (one with $p_T > 1$ GeV, the other with $p_T > 0.5$ GeV) and $\geqslant 1$ SMT hits are inside the $\Delta R < 0.5$ cone defining the jet. The jet taggability is typically 80% in a two-jet sample with an uncertainty of 3%.

For each tagged jet in the simulation, we apply the ratio between the expected taggability times b-tagging efficiency in data and in simulation to reweight the simulated events. For the tagging efficiency of simulated b or c jets, we use $p_T-\eta$ dependent data vs. simulation scale factors, determined from real b jets [19]. In the simulation, the tagged light flavor jets are weighted to reproduce the mistag rate as measured in data using dedicated samples [19].

With the above selection criteria, we observe 137 $W+2$ jet events having exactly one b-tagged jet (ST sample) and 30 events having both jets b-tagged (DT sample). In these samples the multijet background is estimated using as a loose sample the $W+2$ jet ST (DT) sample in which the lepton is selected using the loose lepton-ID criteria. The distribution of the invariant dijet mass of $W+2$ jet events for the ST and DT samples is shown in Fig. 2(a) and (b). The data are compared to the sum of

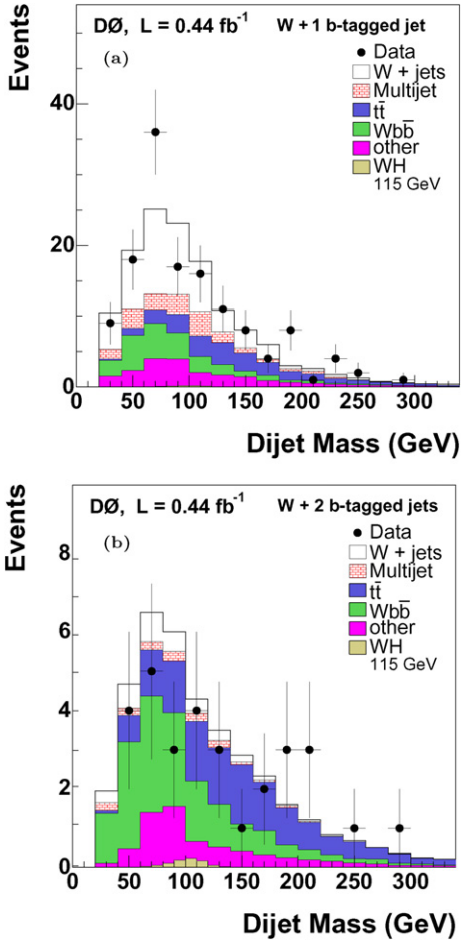

Fig. 2. Dijet mass distributions for the $W+2$ jet events (a) when exactly one jet is tightly b-tagged and (b) when the two jets are loosely b-tagged (see text). The data are compared to $Wb\bar{b}$, $t\bar{t}$, $W+$ jets and other smaller expectations. The background labeled as "other" in the figure is dominated by single top quark production.

the simulated SM processes added to the multijet background. The agreement indicates that the simulation describes the data well.

The different components of the background are shown in Table 1. The small expected contributions from a 115 GeV Higgs are also shown, but no excess above the standard model backgrounds is visible in these distributions, so we proceed to set limits from these distributions, after systematic uncertainty evaluation.

The experimental systematic uncertainties on the efficiencies and those due to the propagation of other systematic uncertainties (trigger, energy calibration, detector response) which affect the signal and SM backgrounds are the following (ranges indicate different values for the e and μ channel): (2–3)% uncertainty from the trigger efficiency, (3–4)% uncertainty for the lepton identification and reconstruction efficiency, (3–4)% for the lepton energy scale and resolution, 5% for the jet identification and reconstruction efficiency, 5% for the modeling uncertainty of the jet multiplicity in the simulation, (5–12)% due to the jet energy calibration uncertainty, 3% for the jet taggability, and (5–6)% for the b-tagging efficiency; for the light

Table 1
Summary table for the ℓ (e and μ) $+2$ jets $+\not\!\!E_T$ final state. Observed events in data are compared to the expected number of $W+2$ jet events before and after b-tagging in the simulated samples of WH, dibosons, $Wb\bar{b}$ production, top production ($t\bar{t}$ and single top), multijet background, and "$W/Z+$jets" production. In the pre-tagged sample the $W/Z+$jets contribution is normalized such that the total expectation is normalized to the data

	$W+2$ jet pre-tagged	$W+2$ jet 1 b-tagged	$W+2$ jet 2 b-tagged
WH	2.3±0.4	0.49±0.07	0.43±0.06
WW, WZ, ZZ	148.7±23.8	5.3±0.8	2.0±0.4
$Wb\bar{b}$	116.3±18.6	22.3±4.4	14.4±3.2
$t\bar{t}$	87.6±8.6	21.0±4.3	12.6±2.7
Single top	41.2±5.3	10.0±4.8	3.7±0.7
Multijet	984±153	22.8±7.5	1.5±0.6
$W/Z+$jets	6908±1076	57.7±10.3	4.1±0.7
Total expect.	8286	139.6±28.5	38.7±5.8
Observed Ev.	8286	137	30

quark jets these uncertainties are 9% (DT) and 13% (ST). In summary, for WH production and simulated backgrounds, the experimental systematic uncertainty is (16–19)%. The multijet background, determined from data, has an uncertainty of 25%. The systematic uncertainty on the cross section of the simulated backgrounds is 6–18%, depending on the process. The uncertainty on the luminosity is 6.1%.

The limits for WH production are obtained using the CL_s method [20,21] taking the dijet invariant mass of the $b\bar{b}$ system as the final discriminating variable. It is performed on the ST and DT samples of the e and μ channels independently (four analyses), which are then combined. The CL_s approach is based on the likelihood ratio test statistic, $Q = L(s+b)/L(b) = \frac{e^{-(s+b)}(s+b)^n}{n!} / \frac{e^{-b}(b)^n}{n!}$, where s and b are the expected numbers of signal and background events while n is the number of data events. For computational ease, the log-likelihood ratio $LLR(n) = -2\ln(Q)$ is used. In order to exploit the shape information of the final discriminating variable, as well as combine the different channels, the LLR values per bin and for all channels are added. Systematic uncertainties are incorporated into the signal and background expectation using Gaussian sampling of individual uncertainties. Correlations between uncertainties across channels are handled by varying simultaneously the fluctuations of identical sources of all channels. The 95% C.L. limits are determined by raising the signal cross sections until the ratio of probabilities for the signal + background hypothesis to the background-only hypothesis falls below 5%.

Fig. 3 shows the LLR distributions for the WH combined result. The LLR values for the signal + background hypothesis (LLR_{s+b}), background-only hypothesis (LLR_b), and the observed data (LLR_{obs}) are shown. The quantities LLR_{s+b}, LLR_b, and LLR_{obs} are obtained by setting $n = s+b$, b or n(observed) into $LLR(n)$. The shaded bands represent the one and two standard deviation (σ) departures for LLR_b. These distributions can be interpreted as follows: The separation between LLR_b and LLR_{s+b} provides a measure of the discriminating power of the search; the width of the LLR_b distribution provides an estimate of the sensitivity of the analysis to a

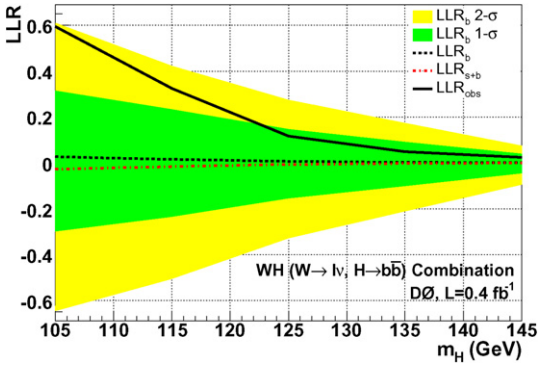

Fig. 3. LLR distributions obtained with the CL_s method for the combination of the ST and DT samples in the WH channel.

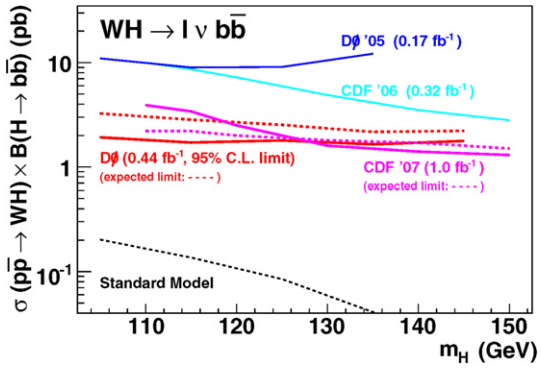

Fig. 4. 95% C.L. cross section upper limit (and corresponding expected limit) on $\sigma(p\bar{p} \to WH) \times B(H \to b\bar{b})$ (W boson decaying into a lepton + neutrino and Higgs boson into $b\bar{b}$) vs. Higgs boson mass, compared to the SM expectation. The published D0 e channel observed results, based on an integrated luminosity of 0.17 fb^{-1} and the CDF ($e + \mu$ channels) results with 0.32 fb^{-1} and 1.0 fb^{-1} are also shown.

signal-plus-background-like fluctuation in data, taking account of the systematic uncertainties; the value of LLR_{obs} relative to LLR_{s+b} and LLR_b indicates whether the data distribution appears to be more signal-like or background-like, and the significance of any departures of LLR_{obs} from LLR_b can be evaluated by the width of the LLR_b distribution.

The observed (expected) combined upper limits obtained at 95% C.L. on $\sigma(p\bar{p} \to WH) \times B(H \to b\bar{b})$ range from 1.6 pb to 1.9 pb (2.2 pb to 3.3 pb) for Higgs boson masses between 105 and 145 GeV and are displayed in Fig. 4. They are also given in Table 2 together with the ST and DT subchannel limits and the ratios of all these limits to the predicted SM cross section. These new WH upper limits are compared in Fig. 4 to the previously published results on WH production from D0 on 0.17 fb^{-1} of data in the electron channel only [1] and CDF (0.32 fb^{-1} $e + \mu$ channels) [2]. The improvement in sensitivity obtained with this analysis is clearly visible in the region where the Tevatron is most sensitive to a Higgs boson with mass in the 115–135 GeV range. The result is also compared to the latest results from the CDF Collaboration on 1.0 fb^{-1} of data [3], showing comparable expected sensitivity when taking into account the difference in integrated luminosity.

With the limits from the WH channels reported above, we now turn to the combination of these with limits previously obtained from other channels. We combine our new WH results with all the other direct searches for SM Higgs bosons published by DØ. These are searches for Higgs bosons produced in association with vector bosons ($p\bar{p} \to ZH \to \nu\bar{\nu}b\bar{b}/\ell\ell b\bar{b}$ [4,5], $p\bar{p} \to WH \to WWW$ [6]) or singly through gluon–gluon fusion ($p\bar{p} \to H \to WW$ [7]). The searches were conducted with data collected during the period 2003–2005 and correspond to integrated luminosities ranging from 0.30 fb^{-1} to 0.45 fb^{-1}. They are separated into twelve final states (adding to the four WH final states combined earlier) and referred to as analyses in the following. Each analysis is designed to isolate a particular final state defined by a Higgs boson production and decay mode. To ensure proper combination of signals, the analyses were designed to be mutually exclusive.

The sixteen analyses are categorized by their production processes and outlined in Table 3. When possible, we search for both $H \to b\bar{b}$ and $H \to WW$ decays. For the $H \to b\bar{b}$ decays, we conduct separate ST and DT analyses, except for $ZH \to \ell^+\ell^- b\bar{b}$ analyses where only the DT analysis has been performed. The decays of the vector bosons further define the analyzed final states: $WH \to e\nu b\bar{b}$, $WH \to \mu\nu b\bar{b}$, $ZH \to ee b\bar{b}$,

Table 2
Observed and expected 95% C.L. limits on the cross section times branching fraction $\sigma \times B$, where $B = B(H \to b\bar{b})$ and σ is in pb, for different Higgs boson mass values, for single and double b-tagged events, and ST + DT combination in the $WH \to \ell\nu b\bar{b}$ channel, with $\ell = e$ or μ. The corresponding ratios to the predicted SM Higgs production cross section are also given

WH / Higgs mass [GeV]	105	115	125	135	145
ST observed $\sigma \times B$	6.62	5.74	5.17	4.79	4.74
ST expected $\sigma \times B$	8.11	6.94	6.10	4.90	5.08
DT observed $\sigma \times B$	2.21	2.12	2.25	1.98	1.97
DT expected $\sigma \times B$	3.55	3.07	2.89	2.43	2.58
ST + DT observed $\sigma \times B$	1.92	1.71	1.79	1.64	1.77
ST + DT expected $\sigma \times B$	3.25	2.83	2.53	2.16	2.21
ST observed ratio to SM	34.9	44.9	65.5	112.8	250.7
ST expected ratio to SM	42.8	54.4	77.3	115.4	268.5
DT observed ratio to SM	11.7	16.6	28.5	46.6	104.1
DT expected ratio to SM	18.8	24.1	36.6	57.3	136.6
ST + DT obs. ratio to SM	10.1	13.4	22.6	38.6	93.4
ST + DT exp. ratio to SM	17.1	22.1	32.0	51.0	116.7

Table 3
List of analysis channels, corresponding integrated luminosities (L), final variables for the search, and references. LH stands for likelihood

Channel	L (fb^{-1})	Final variable	Ref.
$WH \to e\nu b\bar{b}$, ST/DT	0.43	Dijet mass	–
$WH \to \mu\nu b\bar{b}$, ST/DT	0.45	Dijet mass	–
$WH \to \not{\ell}\nu b\bar{b}$, ST/DT	0.30	Dijet mass	[4]
$ZH \to \nu\bar{\nu}b\bar{b}$, ST/DT	0.30	Dijet mass	[4]
$ZH \to \mu\mu b\bar{b}$, DT	0.37	Dijet mass	[5]
$ZH \to ee b\bar{b}$, DT	0.45	Dijet mass	[5]
$WH \to WWW$ ($e^\pm e^\pm$)	0.45	LH discriminant	[6]
$WH \to WWW$ ($e^\pm \mu^\pm$)	0.43	LH discriminant	[6]
$WH \to WWW$ ($\mu^\pm \mu^\pm$)	0.42	LH discriminant	[6]
$H \to WW$ (ee)	0.33	$\Delta\varphi(e, e)$	[7]
$H \to WW$ ($e\mu$)	0.32	$\Delta\varphi(e, \mu)$	[7]
$H \to WW$ ($\mu\mu$)	0.30	$\Delta\varphi(\mu, \mu)$	[7]

$ZH \to \mu\mu b\bar{b}$, and $ZH \to \nu\bar{\nu}b\bar{b}$. There is a sizeable amount of $WH \to \ell\nu b\bar{b}$ signal that can mimic the $ZH \to \nu\bar{\nu}b\bar{b}$ final state when the lepton is undetected, or when the lepton is a τ decaying hadronically. This case is treated as a separate WH analysis, referred to as $WH \to \not{\ell}\nu b\bar{b}$.

We also include the analysis of $WH \to WWW$ final states when the associated W boson and the same-charged W boson from the Higgs boson decay leptonically, thus defining six final states: $WH \to We^{\pm}\nu e^{\pm}\nu$, $We^{\pm}\nu\mu^{\pm}\nu$, and $W\mu^{\pm}\nu\mu^{\pm}\nu$, which are then grouped into three analyses: $e^{\pm}e^{\pm}$, $\mu^{\pm}\mu^{\pm}$, and $e^{\pm}\mu^{\pm}$. All decays of the third W boson are included.

In the case of $p\bar{p} \to H \to WW$ production, we again search for leptonic W boson decays with three final states, $WW \to e\nu e\nu$, $e\nu\mu\nu$, and $\mu\nu\mu\nu$. For the gluon–gluon fusion process, $H \to b\bar{b}$ decays are not considered due to the large multijet background.

As before, we combine results using the CL_s method. Systematic uncertainties are treated as uncertainties on the expected numbers of signal and background events, not on the outcomes of the limit calculations. This approach ensures that the uncertainties and their correlations are propagated to the outcome with their proper weights. The method used here utilizes binned final-variable distributions rather than a single-bin (fully-integrated) value. In the case of the $H \to b\bar{b}$ analyses, the final variable used for limit setting is the invariant dijet mass, as shown for the WH channel in Fig. 2. In the case where $H \to WW$, the Higgs mass cannot be directly reconstructed due to the neutrinos in the final state. Thus, the $WH \to WWW$ analysis uses a likelihood (LH) discriminant formed from topological variables as a final variable [6], while the $p\bar{p} \to H \to WW$ analysis uses the separation in φ between the final state leptons $\Delta\varphi(\ell_1, \ell_2)$ [7]. Each signal and background final variable is smoothed via Gaussian kernel estimation [22].

Both signal and background systematic uncertainties vary for the different analyses. Here we summarize only the largest contributions, referring to the original publications for details. All analyses carry an uncertainty on the integrated luminosity of 6.1%. The $H \to b\bar{b}$ analyses have an uncertainty on the b-tagging rate of (5–7)% per tagged jet. These analyses also have an uncertainty on the jet energy calibration and acceptances of 8–10%. For the $H \to WW$ and $WH \to WWW$ analyses, the largest experimental uncertainties are associated with lepton measurement and acceptances. These values range from (3–8)% depending on the final state. The largest contribution for all analyses is the uncertainty on the background cross sections at (6–19)% depending on the background. The uncertainty on the expected multijet background is dominated by the statistics of the data sample from which it is estimated, hence is uncorrelated between analyses. The systematic uncertainties for the background rates are generally several times larger than the signal expectation itself and are thus an important factor in the calculation of limits. As such, each systematic uncertainty is folded into the signal and background expectations via Gaussian distribution. Correlations between systematic sources are carried through in the calculation. All systematic uncertainties originating from a common source, see Table 4, are taken to be correlated.

Table 4
List of leading correlated systematic uncertainties. The values for the systematic uncertainties are the same for the $ZH \to \nu\bar{\nu}b\bar{b}$ and $WH \to \not{\ell}\nu b\bar{b}$ channels. Each uncertainty is considered to be 100% correlated across channels. The correlated systematic uncertainty on the background cross section (σ) is itself subdivided according to the different background processes in each analysis

Source	$WH, e\nu b\bar{b}$ DT(ST)	$WH, \mu\nu b\bar{b}$ DT(ST)	WW, WWW
Luminosity (%)	6	6	6
Jet Calibration (%)	4	5	3
Jet ID (%)	7	7	0
Electron ID (%)	7	0	2
Muon ID (%)	0	5	8
b-tagging (%)	9(5)	9(5)	0
Background σ (%)	6–19	6–19	6–19
Source	$ZH \to \nu\bar{\nu}b\bar{b}$ DT(ST)	$ZH \to eeb\bar{b}$	$ZH \to \mu\mu b\bar{b}$
Luminosity (%)	6	6	6
Jet Calibration (%)	6	7	7
Jet ID (%)	7	7	5
Electron ID (%)	0	8	0
Muon ID (%)	0	0	12
b-tagging (%)	10(7)	12	12
Background σ (%)	6–19	6–19	6–19

To minimize the effect of systematic uncertainties on the search sensitivity, the individual background contributions are fitted to the data observation by minimizing a profile likelihood function [21]. The fit computes the optimal central values for the systematic uncertainties, while accounting for departures from the nominal predictions by including a term in the χ^2 function which sums the squared deviation of each systematic uncertainty in units normalized by its $\pm 1\sigma$ uncertainties. A fit is performed to the background-only hypothesis and is constrained to bins with a signal expectation smaller than 4% of the total expected background.

To set limits on Higgs boson production ($\sigma \times B(H \to X)$) the sixteen analyses are first grouped by final state to produce individual results. We then group channels by production modes to form combined results and study their respective sensitivities. The individual analyses are grouped to form the LLR distributions shown in Fig. 5 for (a) all WH searches, with $H \to b\bar{b}$ (ST, DT) in the low mass range ($m_H =$ 105–145 GeV), (b) all ZH searches (ST, DT) in the same low mass range, (c) all $WH \to WWW$ searches, over an extended mass range ($m_H =$ 120–200 GeV), and (d) all $H \to WW$ searches, over the full mass range ($m_H =$ 100–200 GeV). We then combine groups (a)–(d) over the full mass range, as shown in Fig. 6.

We also compute our results in terms of the ratio of the limits to the SM cross section $\sigma \times B(H \to X)$ as a function of Higgs boson mass. The SM prediction for Higgs boson production would therefore be excluded at 95% C.L. when this limit ratio falls below unity. Table 5 shows the expected and observed 95% C.L. cross section limits and their ratios to the SM for the WH and ZH analyses in the mass range $m_H =$ 105–145 GeV. Table 6 shows the same information for $WH \to WWW$ and $H \to WW$ over the full mass range. The ratios to the SM obtained with the full combination are also given and show the

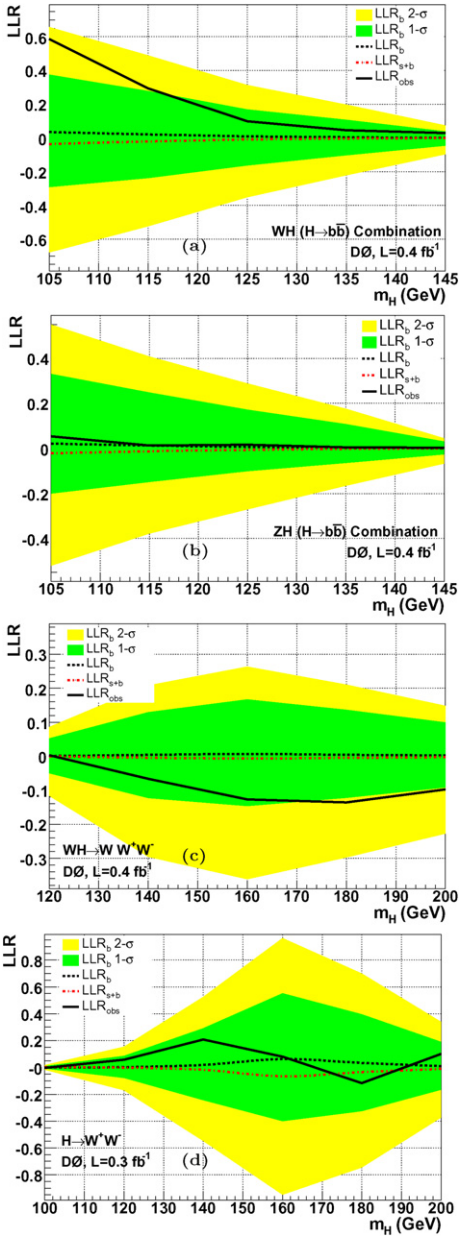

Fig. 5. LLR distributions obtained with the CL_s method for the associated production of (a) $WH(H \to b\bar{b})$, (b) $ZH(H \to b\bar{b})$, (c) $WH(H \to WW)$, and (d) for the direct production channel, $H \to WW$. See text for details.

gain obtained by using the full information, compared to the individual channels.

The expected limits for the cross section times branching fraction for the four groups of analyses (a)–(d) and for the full combination, relative to the SM expectations, are shown in Fig. 7. For the full combination of all analyses, the expected and observed cross section times branching ratio, relative to those for the SM, are shown in Fig. 8. Compared to an earlier simulation study of the Higgs boson search sensitivity conducted prior to Tevatron Run II [23], our current analyses have added new channels, have extended the mass range, and show a more uniform sensitivity for $110 < m_H < 190$ GeV.

In summary, we have presented new 95% C.L. limits on the $WH \to e/\mu\nu b\bar{b}$ production cross section times branching fraction which range from 1.6 to 1.9 pb for $105 < m_H < 145$ GeV. For comparison, the expected SM cross section for $m_H = 115$ GeV is 0.13 pb.

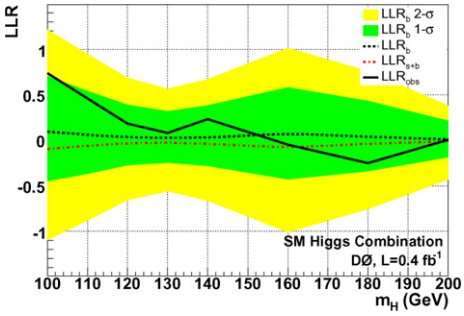

Fig. 6. LLR distributions obtained with the CL_s method for the combination of all channels. See text for details.

Table 5
Observed and expected 95% C.L. upper limits on the cross section times branching fraction $\sigma \times B$, where $B = B(H \to b\bar{b})$, and σ is in pb, for different Higgs boson mass values, for the WH and ZH combined channels (WH includes the leptonic channels, and the case where the charged lepton is not detected; ZH includes the ee, $\mu\mu$, and $\nu\nu$ channels)

Higgs mass [GeV]	105	115	125	135	145
WH observed $\sigma \times B$	1.60	1.49	1.57	1.56	1.65
WH expected $\sigma \times B$	2.83	2.38	2.22	1.89	2.17
ZH observed $\sigma \times B$	2.41	2.23	1.97	1.77	3.21
ZH expected $\sigma \times B$	2.21	2.02	1.73	1.52	2.65
WH observed ratio to SM	8.4	11.7	19.8	36.7	87.2
WH expected ratio to SM	14.9	18.6	28.1	44.5	114.7
ZH observed ratio to SM	21.1	28.5	40.0	66.0	263.6
ZH expected ratio to SM	19.4	25.9	35.2	56.6	217.4

We have then combined these results with all previously published Higgs boson searches by the D0 collaboration obtained with a similar luminosity (between 0.30 and 0.45 fb^{-1}) to form new limits more sensitive than each individual limit. The combined observed (expected) 95% C.L. limit ratios to SM cross sections for $p\bar{p} \to WH$, $H \to b\bar{b}$ range from 11.7 (18.6) at $m_H = 115$ GeV to 36.7 (44.5) at $m_H = 135$ GeV. The combined observed (expected) 95% C.L. limit ratios to SM cross sections for $p\bar{p} \to ZH$, $H \to b\bar{b}$ range from 28.5 (25.9) at $m_H = 115$ GeV to 66.0 (56.7) at $m_H = 135$ GeV. The fully combined observed (expected) 95% C.L. limit ratio to the SM cross sections are 8.5 (12.1) at $m_H = 115$ GeV, 10.2 (9.0) at $m_H = 160$ GeV, and 23.7 (23.5) at $m_H = 200$ GeV.

These limits and ratios will decrease in the near future with the additional luminosity recorded at the Tevatron; more than 2 fb^{-1} are currently being analyzed. New techniques are being developed to improve the sensitivity through advanced multivariate techniques, neural-network b-tagging, and improved di-jet mass resolution. In addition, an anticipated combination with the results from the CDF collaboration would yield an increase in sensitivity of about 40%. With the total expected integrated luminosity (6–8 fb^{-1}), the Tevatron is expected to provide sensitivity to the standard model Higgs boson beyond the current LEP limit [24].

Table 6
Observed and expected 95% C.L. upper limits on the cross section times branching fraction $\sigma \times B$, where $B = B(H \to WW)$ and σ is in pb, for different Higgs boson mass values, for $WH \to WWW$ and $H \to WW$. The ratios to the predicted values of the SM Higgs production cross section for these channels and for the full D0 combination, are also given

Higgs mass [GeV]	100	110	115	120	130	140	160	180	200
$WH \to WWW$ observed $\sigma \times B$	–	–	–	11.27	4.41	1.57	0.09	0.010	0.004
$WH \to WWW$ expected $\sigma \times B$	–	–	–	10.78	3.53	1.30	0.07	0.007	0.003
$H \to WW$ observed $\sigma \times B$	10.79	5.61	–	6.07	5.94	4.24	3.69	4.07	3.25
$H \to WW$ expected $\sigma \times B$	8.94	6.31	–	7.74	6.18	5.25	3.58	3.40	3.98
$WH \to WWW$ observed ratio to SM	–	–	–	110.7	74.7	53.7	46.1	62.1	89.6
$WH \to WWW$ expected ratio to SM	–	–	–	105.9	59.8	44.7	34.4	44.6	60.8
$H \to WW$ observed ratio to SM	636.4	98.9	–	46.1	26.4	14.0	9.9	15.4	22.2
$H \to WW$ expected ratio to SM	527.5	111.2	–	58.8	27.4	17.3	9.6	12.8	27.2
D0 observed ratio to SM	5.5	7.1	8.5	10.5	14.2	12.8	10.2	16.1	23.7
D0 expected ratio to SM	8.7	10.8	12.1	14.3	15.7	13.8	9.0	12.1	23.5

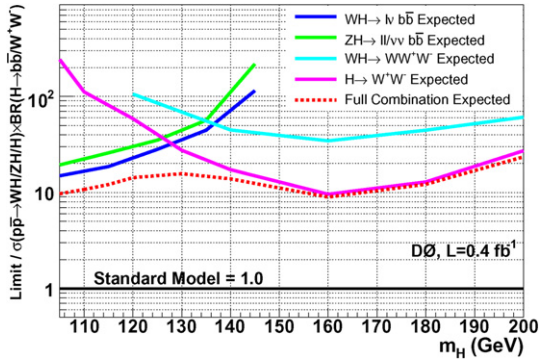

Fig. 7. Ratios of the expected limit on the Higgs boson production cross section times branching fraction to the SM expectation, for the different channel groups and for the full D0 combination.

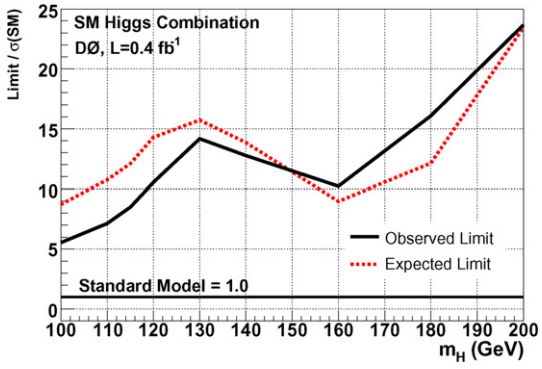

Fig. 8. Ratios of the expected and observed limit on the Higgs boson production cross section times branching fraction to the SM expectation, for the full D0 combination.

Acknowledgements

We thank the staffs at Fermilab and collaborating institutions, and acknowledge support from the DOE and NSF (USA); CEA and CNRS/IN2P3 (France); FASI, Rosatom and RFBR (Russia); CAPES, CNPq, FAPERJ, FAPESP and FUNDUNESP (Brazil); DAE and DST (India); Colciencias (Colombia); CONACyT (Mexico); KRF and KOSEF (Korea); CONICET and UBACyT (Argentina); FOM (The Netherlands); Science and Technology Facilities Council (United Kingdom); MSMT and GACR (Czech Republic); CRC Program, CFI, NSERC and WestGrid Project (Canada); BMBF and DFG (Germany); SFI (Ireland); The Swedish Research Council (Sweden); CAS and CNSF (China); Alexander von Humboldt Foundation.

References

[1] D0 Collaboration, V.M. Abazov, et al., Phys. Rev. Lett. 94 (2005) 091802.
[2] CDF Collaboration, D. Acosta, et al., Phys. Rev. Lett. 94 (2005) 091802.
[3] CDF Collaboration, T. Aaltonen, et al., Phys. Rev. Lett. 100 (2008) 041801.
[4] D0 Collaboration, V.M. Abazov, et al., Phys. Rev. Lett. 97 (2006) 161803.
[5] D0 Collaboration, V.M. Abazov, et al., Phys. Lett. B 655 (2007) 209.
[6] D0 Collaboration, V.M. Abazov, et al., Phys. Rev. Lett. 97 (2006) 151804.
[7] D0 Collaboration, V.M. Abazov, et al., Phys. Rev. Lett. 96 (2006) 011801.
[8] D0 Collaboration, V.M. Abazov, et al., Erratum to Phys. Rev. Lett. 94 (2005) 151801, Phys. Rev. Lett., in press.
[9] D0 Collaboration, V.M. Abazov, et al., Nucl. Instrum. Methods A 338 (1994) 185.
[10] D0 Collaboration, V.M. Abazov, et al., Nucl. Instrum. Methods A 565 (2006) 463.
[11] D0 Collaboration, V.M. Abazov, et al., Phys. Rev. D 76 (2007) 092007.
[12] T. Sjostrand, et al., Comput. Phys. Commun. 135 (2001) 238.
[13] H.L. Lai, et al., Phys. Rev. D 55 (1997) 1280.
[14] A. Pukhov, et al., hep-ph/9908288.
[15] M. Mangano, et al., hep-ph/0206293.
[16] J. Campbell, K. Ellis, MCFM, Montecarlo for FeMtobarn processes, http://mcfm.fnal.gov/.
[17] R. Brun, F. Carminati, CERN Program Library Long Writeup W5013, 1993, unpublished.
[18] G. Blazey, et al., in: U. Baur, R.K. Ellis, D. Zeppenfeld, (Eds.), Proceedings of the workshop QCD and Weak Boson Physics in Run II, Batavia, 2000, p. 47.
[19] S. Greder, *b* quark tagging and cross-section measurement in quark pair production at DØ, FERMILAB-THESIS-2004-28, 2004.
[20] T. Junk, Nucl. Instrum. Methods A 434 (1999) 435.
[21] W. Fisher, FERMILAB-TM-2386-E, 2007.
[22] K.S. Cranmer, Comput. Phys. Commun. 136 (2001) 198, hep-ph/0011057.
[23] M. Carena, et al., hep-ph/0010338.
[24] ALEPH Collaboration, DELPHI Collaboration, L3 Collaboration, OPAL Collaboration, The LEP Working Group for Higgs Boson Searches, Phys. Lett. B 565 (2003) 61.